

Analytical analysis of Lyot coronagraphs response

André Ferrari

LUAN, Université de Nice Sophia-Antipolis, Parc Valrose, 06108 Nice cedex 02, France

ABSTRACT

We derive an analytical solution to the computation of the output of a Lyot coronagraph for a given complex amplitude on the pupil plane. This solution, which does not require any simplifying assumption, relies on an expansion of the entrance complex amplitude on a Zernike base. According to this framework, the main contribution of the paper is the expression of the response of the coronagraph to a single base function. This result is illustrated by a computer simulation which describes the classical effect of propagation of a tip-tilt error in a coronagraph.

Subject headings: instrumentation: adaptive optics – techniques: high angular resolution

1. Introduction

The discovery of extrasolar planets is at the origin of a renewed interest in stellar coronagraphy. Considering the ambition of the targeted objectives, many authors have pointed out the necessity for a very accurate analysis of the system in order to study various undesired effects. For example, the specific properties of the light intensity measured by a system based on an extreme adaptive optics system and a coronagraph are the result that neither the residuals of the turbulence, nor the ideal coronagraphed point-spread function can be neglected with respect to the faint object (planet). Aime and Soummer (2004) analyzed the fact that the wavefront amplitudes associated to these two contributions will interfere leading to the so-called “pinned” speckles. Another example is given by Lloyd and Sivaramakrishnan (2005) which pointed out that a small misalignment of the star with the center of the stop can result in a fake source. A related problem is also present in (Soummer 2004) which derives the optimal apodization for an arbitrary shaped aperture using an algorithm proposed independently in (Guyon and Roddier 2000) which relies on iterated simulations of the coronagraph response.

More generally, an intense activity aims to optimize the different coronagraph parameters (mask size, apodization shape,...) for a number of projects dedicated to devise high-dynamic range imaging on the VLT (Sphere), Gemini (GPI) or the Subaru telescope (HiCIAO), see for example (Aime and Vakili 2006). The input/output relation of a coronagraph is in this case simulated by numerical computations based on discrete Fourier transforms. However, such a numerical technique suffers from the well-known problems related to the choice of the extent of the sampled surface and

the sampling frequency which both define the sampling in the transformed domain. Note that this compromise is coupled with the difficulty to evaluate numerically the simulation errors.

This work focuses on the analytical characterization of the response of a Lyot coronagraph. The objective is obviously also to gain deeper insight in the behaviour of the system. This problem has already been studied in the literature and analytical results were obtained under various assumptions. In the one-dimensional case, Lloyd and Sivaramakrishnan (2005) assume that the Lyot stop is band limited and the phase on the telescope aperture is small. This last hypothesis is removed in (Sivaramakrishnan et al. 2005) where the computation is carried for a rectangular pupil assuming again that the Lyot stop is band-limited. The development presented herein for a circular pupil differs from these approaches substituting these simplifying assumptions by an expansion of the complex amplitude on an orthogonal basis.

Section 1 recalls the general formalism of Lyot coronagraphy and justifies the choice of an expansion of the complex amplitude on a Zernike base. Section 2 contains the main results of the paper; the response of the coronagraph to a Zernike polynomial is computed. The result involving an infinite sum, a bound on the truncation error is then derived. Section 3 presents two simulations. First the response of the coronagraph to the 6 first Zernike functions is computed. Then the formalism derived in this paper is used to illustrate the effect of a tip-tilt error in a coronagraph. A short appendix containing the material required for the mathematical derivations of section 2 is included at the end of the paper.

2. Notations and hypothesis

2.1. Coronagraph formalism

We follow the notations of Aime et al. (2002) and Soummer et al. (2003). The successive planes of the coronagraph are denoted by A , B , C and D . A is the entrance aperture, B denotes the focal plane with the mask (without loss of generality we assume that the amplitude of the mask is $1 - \epsilon$ where $\epsilon = 1$ corresponds to the classical Lyot coronagraph and $\epsilon = 2$ to the Roddier coronagraph), C is the image of the aperture with the Lyot stop and D is the image in the focal plane after the coronagraph. The aperture transmission function is $p(x, y)$ and the wavefront complex amplitude in A is $\Psi(x, y)$. In the case of an apodized pupil, we assume that the apodization function is included in $\Psi(x, y)$. In order to simplify the notations, the mask function in B is defined with coordinates proportional to $1/\lambda f$ and decomposed as:

$$1 - \epsilon m\left(\frac{x}{\lambda f}, \frac{y}{\lambda f}\right) \quad (1)$$

where function $m(\cdot)$ equals to 1 inside the coronagraphic mask and 0 outside.

We will make in the sequel the usual approximations of paraxial optics. Moreover we neglect the quadratic phase terms associated with the propagation of the waves or assume that the optical

layout is properly designed to cancel it (Aime 2003). The expression in cartesian coordinates of the complex amplitude in the successive planes are:

$$\Psi_A(x, y) = \Psi(x, y)p(x, y) \quad (2)$$

$$\Psi_B(x, y) = \frac{1}{j\lambda f} \widehat{\Psi}_A \left(\frac{x}{\lambda f}, \frac{y}{\lambda f} \right) \left(1 - \epsilon m \left(\frac{x}{\lambda f}, \frac{y}{\lambda f} \right) \right) \quad (3)$$

$$\Psi_C(x, y) = \frac{1}{j\lambda f} \widehat{\Psi}_B \left(\frac{x}{\lambda f}, \frac{y}{\lambda f} \right) p(-x, -y) \quad (4)$$

$$= -(\Psi_A(-x, -y) - \epsilon [\Psi_A(-u, -v) * \widehat{m}(u, v)](x, y)) p(-x, -y) \quad (5)$$

$$\begin{aligned} \Psi_D(x, y) &= \frac{-1}{j\lambda f} \widehat{\Psi}_A \left(\frac{-x}{\lambda f}, \frac{-y}{\lambda f} \right) \\ &\quad + \epsilon \frac{1}{j\lambda f} \left(\widehat{\Psi}_A(-x, -y) m(-x, -y) * \widehat{p}(-x, -y) \right) \left(\frac{x}{\lambda f}, \frac{y}{\lambda f} \right) \end{aligned} \quad (6)$$

where \widehat{f} is the Fourier transform of f and $*$ denotes convolution. Eqs. (5,6) assume that the Lyot stop is the same as the pupil. However for classical “unapodized” Lyot coronagraph the residual intensity in plane C is concentrated at the edges of the pupil and a reduction of the Lyot stop size is needed in order to improve the rejection. The case of a reduced Lyot stop, which consists in convolving Eq. (6) by the appropriate function, has not been considered in Eqs. (5,6) to alleviate the notations but will be discussed in section 3. It is important to note that the reduction of the Lyot stop can be avoided using a prolate apodized entrance pupil which will optimally concentrate the residual amplitude in C , see for example (Aime et al. 2002).

The coronagraph response being derived herein for a circular pupil, the use of polar coordinates will be preferred. Transcription of previous equations to polar coordinates is straightforward. Moreover, as long as the aperture transmission function and the stop have a circular symmetry, their Fourier transform will verify the same symmetry, as proved by Eq. (A3) with $m = 0$, i.e. the Hankel transform. This leads to the following expression of the complex amplitude in D :

$$\Psi_D(r\lambda f, \theta) = \frac{-1}{j\lambda f} \widehat{\Psi}_A(r, \theta + \pi) + \frac{\epsilon}{j\lambda f} \left(\left(\widehat{\Psi}_A(r, \theta + \pi) m(r) \right) * \widehat{p}(r) \right) (r, \theta) \quad (7)$$

where the convolution of the two functions is still computed with respect to the cartesian coordinates (x, y) .

2.2. Choice of a base

As mentioned in the introduction, the analytical computation of the coronagraph response proposed herein relies on the expansion of the complex amplitude in A on an orthogonal basis. Eq. (7) shows that the coronagraph *acts linearly* on the complex amplitude, consequently the problems simplifies to the computation of the response of each basis function. The retained solution consists in the expansion of the complex amplitude in A on Zernike polynomials. Basic properties of the Zernike polynomials required in the paper are recalled in appendix A.

Adopting the usual ordering of the Zernike circle polynomial (Mahajan 1994) we can write:

$$\Psi_A(r, \theta) = \sum_{(m,n)} a_{(m,n)} U_n^m(r/R, \theta) \quad (8)$$

$$= \sum_k a_k Z_k(r/R, \theta), \quad a_k \equiv a_{(m,n)} \in \mathbb{C} \quad (9)$$

where R is the radius of the aperture. This expansion is rather unusual, the Zernike polynomials being generally used for the expansion of the wavefront. However it is worthy to note that, as Eq. (5) shows, a coronagraphic system will always introduce amplitude aberration. Hence, even in the case of a perfect wave with no aberration in A , an expansion of only the phase in C will not be appropriate. Finally, Eq. (9) can also be justified by the fact that it coincides (up to a linear transform) with the classical approximation of the complex amplitude in the case of sufficiently small phase errors assuming a first order development of the exponential function.

We will illustrate the expansion (9) in the case of tip-tilt error with an apodized pupil:

$$\Psi_A(r, \theta) = a(r) \Pi(r) e^{j\beta r \cos(\theta)} \quad (10)$$

where $a(r)$ denotes the pupil apodization and $\Pi(r) = 1$ for $r \in [0, 1)$ and 0 if $r \geq 1$. Computation of the projection of $\Psi_A(r, \theta)$ on $U_n^m(r/R, \theta)$ is straightforward using the definition of the Bessel functions of integer order (Abramowitz and Stegun 1972):

$$a_k = R^2 \int_0^1 \int_0^{2\pi} R_n^m(r) \cos(m\theta) a(r) e^{j\beta r \cos(\theta)} r dr d\theta \quad (11)$$

$$= 2\pi R^2 j^m \int_0^1 a(r) R_n^m(r) J_m(\beta r) r dr \quad (12)$$

The projection of $\Psi_A(r, \theta)$ on $U_n^{-m}(r/R, \theta)$ equals 0.

- In the unapodized case, $a(r) = 1$, integral in Eq. (12) can be computed using Eq. (A2):

$$a_k = 2\pi R^2 j^m (-1)^{\frac{n-m}{2}} \frac{J_{n+1}(\beta)}{\beta} \quad (13)$$

- A particularly important case is that where $a(r)$ is proportional to the circular prolate function $\varphi_{0,0}(c, rR)$, (Soummer et al. 2003). In this case the integral in Eq. (12) can be computed using the expansion of $\varphi_{0,0}(c, r)$ derived in (Slepian 1964):

$$\varphi_{0,0}(c, r) = \sum_{k=0}^{\infty} d_k^{0,0}(c) \sqrt{r} F(k+1, -k; 1; r^2) \quad (14)$$

The function $F(k+1, -k; 1; r^2)$ defined in Eq. (A8) reduces to a polynomial of order $2k$ which, as mentioned in (Slepian 1964) “is closely related to the Zernike polynomials”. Indeed using Eq. (A7) and the results below it can be easily checked that: $F(k+1, -k; 1; r^2) = (-1)^k R_{2k}^0(r)$.

Inserting this expansion in Eq. (12) and integrating terms by terms leads to integrals which generalize Eq. (A2). These integrals can be computed for example using of integrals of the type $\int_0^1 r^\nu J_m(\beta r) dr$ (Gradshteyn et al. 2000). This derivation will not be presented herein for sake of brevity.

Finally, for more complicated complex amplitudes, the a_k can be of course computed numerically. This problem as been addressed in (Pawlak and Liao 2002) using a piecewise approximation of $\Psi_A(x, y)$ over a lattice of squares with size $\Delta \times \Delta$ and centered on point (x_i, y_j) . In this case the estimation of a_k is given by:

$$\hat{a}_k = \sum_{(x_i, y_j) \in \mathcal{D}} \Psi_A(x_i, y_j) w_n^m(x_i, y_j)^* \quad (15)$$

where $w_n^m(x_i, y_j)$ is the integral of the Zernike polynomial $U_n^m(\rho/R, \phi)$ over the square centered on (x_i, y_j) . (Pawlak and Liao 2002) gives bound for the mean integrated squared error on the reconstruction of $\Psi_A(x, y)$ when the coefficients are given by Eq. (15). This analysis is particularly important in our case because it quantifies the dependence of the error on the smoothness of $\Psi_A(x, y)$, the sampling rate Δ and the geometrical error due to the circular geometry of the pupil.

3. Coronagraph response

3.1. Response of the coronagraph to a Zernike polynomial

The purpose of this section is to compute the complex amplitude in D when the complex amplitude in A is the Zernike polynomial with radial degree n and azimuthal frequency m . In this case the complex amplitude $\Psi_D(r, \theta)$ will be denoted as $\mathcal{D}_n^m(r, \theta)$. According to Eq. (7), the difficulty in the computation of $\mathcal{D}_n^m(r, \theta)$ lies in the evaluation of the convolution:

$$\Xi(r, \theta) = \left(\left(\widehat{\Psi}_A(r, \theta + \pi) m(r) \right) * \widehat{p}(r) \right) (r, \theta) \quad (16)$$

In this expression $m(r)$ is an “annular” mask of radius d which, with the definition adopted in Eq. (3) is defined as:

$$m(r) = \Pi \left(r \frac{\lambda f}{d} \right) \quad (17)$$

The computation of the convolution in $\Xi(r, \theta)$ is sketched in Fig. 1. Using Eq. (17), $\Xi(r, \theta)$ simplifies to:

$$\Xi(r, \theta) = \int_0^{d/\lambda f} \int_0^{2\pi} \widehat{\Psi}_A(\rho, \phi + \pi) \widehat{p} \left(\sqrt{r^2 + \rho^2 - 2r\rho \cos(\theta - \phi)} \right) \rho d\rho d\phi \quad (18)$$

The next step consists in substituting in this equation:

- $\widehat{p}(r)$ by the Fourier transform of $p(r) = \Pi(r/R)$:

$$\widehat{p}(r) = \frac{RJ_1(2\pi Rr)}{r} \quad (19)$$

- $\Psi_A(\rho, \phi)$ by $U_n^m(\rho/R, \phi)$ and consequently $\widehat{\Psi}_A(\rho, \phi)$ by $R^2\widehat{U}_n^m(rR, \phi)$ where $\widehat{U}_n^m(r, \phi)$ is given in Eq. (A5).

In order to simplify the notations we define the new “standardized” integral $\tilde{\Xi}(r, \theta, \xi)$ by:

$$\tilde{\Xi}(r, \theta, \xi) = \int_0^\xi \int_0^{2\pi} \cos(m\phi) J_{n+1}(\rho) \frac{J_1\left(\sqrt{r^2 + \rho^2 - 2r\rho \cos(\theta - \phi)}\right)}{\sqrt{r^2 + \rho^2 - 2r\rho \cos(\theta - \phi)}} d\rho d\phi \quad (20)$$

It can be easily checked in this case that:

$$\Xi(r, \theta) = R^2 j^m (-1)^{\frac{n-m}{2}} \tilde{\Xi}\left(2\pi Rr, \theta, \frac{2\pi Rd}{\lambda f}\right) \quad (21)$$

Analytical computation of $\tilde{\Xi}(r, \theta, \xi)$ relies on the properties of the Gegenbauer polynomials defined in appendix A. Substituting Eq. (A10) for $\nu = 1$ in Eq. (20) allows indeed to separate the integrations with respect to ρ and ϕ :

$$\tilde{\Xi}(r, \theta, \xi) = 2 \sum_{k=0}^{\infty} (k+1) \frac{J_{k+1}(r)}{r} \int_0^\xi \frac{J_{k+1}(\rho) J_{n+1}(\rho)}{\rho} d\rho \int_0^{2\pi} \cos(m\phi) C_k^{(1)}(\cos(\theta - \phi)) d\phi \quad (22)$$

- Computation of the integral on ϕ is straightforward using (A9):

$$\int_0^{2\pi} \cos(m\phi) C_k^{(1)}(\cos(\theta - \phi)) d\phi = \pi \cos(m\theta) \sum_{q=0}^k \delta(m - k + 2q)$$

- Computation of the integral on ρ relies on recursion formulas on indefinite integrals of products of Bessel functions, (Abramowitz and Stegun 1972):

$$k \neq n, \quad \int_0^\xi \frac{J_n(\rho) J_k(\rho)}{\rho} d\rho = \frac{\xi J_{k-1}(\xi) J_n(\xi) - \xi J_k(\xi) J_{n-1}(\xi) + (n-k) J_n(\xi) J_k(\xi)}{k^2 - n^2} \quad (23)$$

$$\int_0^\xi \frac{J_n(\rho)^2}{\rho} d\rho = \frac{1}{2n} (1 - J_0(\xi)^2 - 2 \sum_{q=1}^{n-1} J_q(\xi)^2 - J_n(\xi)^2) \quad (24)$$

After computation of the integral of Eq. (22), substitution of Eq. (21) in Eq. (7) gives the complex amplitude in D for a single basis function $\Psi_A(r, \theta) = U_n^m(r/R, \theta)$:

$$\mathcal{D}_n^m(r, \theta) = j^{m-1} (-1)^{\frac{n-m}{2}} R \cos(m\theta) \left(-\frac{J_{n+1}(2\pi\mu r)}{r} + \epsilon \sum_{k=0}^{\infty} \eta_{m,n,k}(2\pi\mu d) \frac{J_{k+1}(2\pi\mu r)}{r} \right) \quad (25)$$

with $\mu = R/\lambda f$ and:

$$\eta_{m,n,k}(\xi) = (k+1) \left(\sum_{q=0}^k \delta(m-k+2q) \right) \int_0^\xi \frac{J_{n+1}(\rho) J_{k+1}(\rho)}{\rho} d\rho \quad (26)$$

The corresponding complex amplitude in C for $r < R$ can be directly computed from Eq. (25) using the inverse Fourier transform of $\cos(m\theta) J_{k+1}(2\pi r)/r$ obtained in Eq. (A7):

$$\mathcal{C}_n^m(r, \theta) = (-1)^{\frac{n-m}{2}} \cos(m\theta) \left(-\mathcal{R}_n^m \left(\frac{r}{R} \right) + \epsilon \sum_{k=0}^{\infty} \eta_{m,n,k}(2\pi\mu d) \mathcal{R}_k^m \left(\frac{r}{R} \right) \right) \quad (27)$$

Eqs. (25,27) give an analytical expression of the complex amplitude in C for $r < R$ and in D when a single basis function is applied in A and when the size of the Lyot stop equals the size of the entrance pupil. In the general where the amplitude in A is given by Eqs. (8,9), the complex amplitudes in C and D become:

$$\Psi_C(r, \theta) = \sum_{(m,n)} a_{(m,n)} \mathcal{C}_n^m(r, \theta), \quad \Psi_D(r, \theta) = \sum_{(m,n)} a_{(m,n)} \mathcal{D}_n^m(r, \theta) \quad (28)$$

As mentioned in section 2.1, if the entrance pupil is not apodized a reduction of the Lyot stop must be considered. This is achieved replacing $p(r)$ by $p(\alpha^{-1}r)$ with $\alpha < 1$. The expression of the complex amplitude in C is of course straightforward and for example Eq. (27) becomes $\mathcal{C}_n^m(r, \theta) p(\alpha^{-1}r)$. This result allows numerical computation of the complex amplitude in D using a single Fourier transform. Unfortunately it is much more complicated to obtain an analytical expression of the complex amplitude in D . The derivation presented above can be of course redeveloped replacing $\hat{p}(r)$ by $\alpha^2 \hat{p}(\alpha r)$ and straightforward computation shows that:

1. Similarly to Eq. (25), the convolution (16) will expand in an infinite sum of functions $\cos(m\theta) J_{k+1}(2\pi\alpha\mu r)/r$. However, the ‘‘radial contribution’’ to the coefficients weighting these functions, see Eq. (26), becomes:

$$\int_0^\xi \frac{J_{k+1}(\rho) J_{n+1}(\alpha^{-1}\rho)}{\rho} d\rho$$

which cannot be computed straightforwardly as in Eqs. (23,24).

2. The first term in Eq. (7) is now replaced by the Fourier transform of $U_n^m(\rho/R, \phi) \Pi(r/\alpha R)$ which cannot be anymore calculated using Eq. (A2).

3.2. Bound for the truncation error of $\mathcal{D}_n^m(r, \theta)$

As we are interested in the computation of $\mathcal{C}_n^m(r, \theta)$ or $\mathcal{D}_n^m(r, \theta)$ from the implementation of formula (25), the errors produced when the infinite sum is truncated must be studied. In order to

reduce mathematical developments we only present herein the results for $\mathcal{D}_n^m(r, \theta)$ when the size of the Lyot stop equals the size of the pupil.

We define the truncation error on $\mathcal{D}_n^m(r, \theta)$:

$$\mathcal{E}_N(r, \theta; m, n, \mu, d) = \epsilon R \left| \cos(m\theta) \sum_{k=N+1}^{\infty} \eta_{m,n,k}(2\pi\mu d) \frac{J_{k+1}(2\pi\mu r)}{r} \right| \quad (29)$$

Computation of a bound on the truncation error relies on the classical upper bound for the Bessel functions of integer order (Abramowitz and Stegun 1972):

$$|J_{k+1}(r)| \leq \frac{(r/2)^{k+1}}{k!}, \quad r \geq 0 \quad (30)$$

Substitution of this result in Eq. (26) gives:

$$\eta_{m,n,k}(\xi) \leq (k+1) \left(\sum_{q=0}^k \delta(m-k+2q) \right) \frac{1}{k+n+2} \frac{1}{k!n!} \left(\frac{\xi}{2} \right)^{k+n+2} \quad (31)$$

$$\leq \frac{k+1}{k!n!} \left(\frac{\xi}{2} \right)^{k+n+2} \quad (32)$$

which leads to the following bound for the truncation error:

$$\mathcal{E}_N(r, \theta; m, n, \mu, d) \leq \frac{\epsilon R (\pi\mu)^{3+n} d^{2+n}}{n!} \sum_{k=N+1}^{\infty} \frac{k+1}{(k!)^2} ((\pi\mu)^2 r d)^k \quad (33)$$

The above serie is absolutely convergent for $r > 0$. As a consequence the expansion in Eq. (25) converges uniformly for $(r, \theta) \in [0, \infty) \times [0, 2\pi)$. Finally, it is worthy to note that the computation of the infinite sum in the upper bound (33) can be avoided using the equality:

$$\sum_{k=0}^{\infty} \frac{k+1}{(k!)^2} x^k = I_0(2\sqrt{x}) + \sqrt{x} I_1(2\sqrt{x}) \quad (34)$$

where $I_\nu(x)$ is the modified Bessel function.

4. Simulation results

4.1. Response of the coronagraph to the first Zernike function

Figures 2 and 3 give the intensity in the D plane of the coronagraph when the complex amplitude in the A plane is one of the first six Zernike polynomials. The complex amplitudes have been computed using Eq. (25). Each raw contains $U_n^m(r, \theta)$ and $\mathcal{D}_n^m(r, \theta)$ for a given couple (n, m) . These plots have been obtained truncating the infinite summation of Eq. (25) to the first 40 terms.

The relevance of the truncation error bound is verified in Fig. 4. This plot shows the error bound (33) as a function of r for the parameters used in Figs. 2 and 3. The increase of the bound with r is simply due to the fact that the majoration of $|J_{k+1}(r)|$ given by Eq. (30) is only relevant for small values of r as long as $|J_{k+1}(r)|$ is bounded on $[0, \infty)$. It is important to note that this plot justifies, at least for this configuration, the validity of a truncation to $N = 40$ for the computation of $\mathcal{D}_n^m(r, \theta)$. In this case the truncation error is in fact always less than 10^{-10} .

4.2. Application to tip-tilt error analysis

The effects of a tip-tilt error in Lyot coronagraphs has been extensively studied by Lloyd and Sivaramakrishnan (2005) and Sivaramakrishnan et al. (2005). The scope of the simulation presented here is only to validate the results derived in section 2 simulating the particular case where there is a misalignment of the star with the center of the stop. According to the previous notations the complex amplitude in D decomposes as Eq. (28). In the case of a tip-tilt error in A , the values of the coefficients $a_{(m,n)}$ are given by Eq. (13).

Fig. 5 shows $|\Psi_D(r, \theta)|$ for different values of $\beta > 0$ (the case $\beta = 0$ is given in the first row of Fig. 2). The truncation in the summation (28) has been chosen taking into account that Eq. (13) implies:

$$|a_{(m,n)}| \sim \frac{R^2}{\beta} \sqrt{\frac{2\pi}{n}} \left(\frac{e\beta}{2n}\right)^n, \text{ when } n \rightarrow \infty$$

This simulation illustrates the “transition regime” associated to an interval of locations of the star where the image exhibits a fake structure that could be misinterpreted as a source. See for example in Fig. 5 the results obtained when $\beta = 0.5$ or $\beta = 1$.

5. Conclusion

In this paper we have presented a theoretical formalism for the analytical study of the Lyot coronagraph response. The main purposes of this work are of course to assist coronagraph design but also to improve data processing performances for the detection and characterization of extrasolar planets.

- The first application is the computation of the response of the coronagraph to a planet at a given position. This is achieved for example in the case of a classical Lyot coronagraph using Eqs. (28,13). This point is essential for the derivation of an optimal decision scheme to test the presence of a planet at a given location.
- This formalism can also be applied to fully characterize the statistical properties of the complex amplitude in the D plane. For a given spatial covariance in A which is fixed through the

covariance of coefficients a_k , the spatial covariance in D becomes:

$$\text{cov}[\Psi_D(r, \theta)\Psi_D(r', \theta')] = \sum_{k,l} \text{cov}[a_k, a_l]\mathcal{D}_k(r, \theta)\mathcal{D}_l(r', \theta') \quad (35)$$

Although detection algorithms based solely on the marginal distribution of the complex amplitude can be developed as in (Ferrari et al. 2005), the use of an accurate model for the spatial correlation of the complex amplitude is essential in order to derive detection algorithms with optimal performances, as demonstrated in (Chatelain et al. 2006).

The author thanks the anonymous referee who helped improve the paper. The author is also grateful to Claude Aime and Rémi Soummer for helpful discussions and insightful comments.

A. Appendix

This section presents some facts about Fourier transform in polar coordinates, Zernike and Gegenbauer polynomials.

Among the various available possibilities to define an orthogonal set of functions on the unit radius disk a central position is hold by the Zernike polynomials, see for example (Mahajan 1994) and included references. They are defined for $n \geq m$ by:

$$U_n^m(r, \theta) = R_n^m(r) \cos(m\theta)\Pi(r), \quad U_n^{-m}(r, \theta) = R_n^m(r) \sin(m\theta)\Pi(r) \quad (A1)$$

when n et m share the same parity. The $R_n^m(r)$ are the radial polynomials. Different normalizations exist for $R_n^m(r)$, we retain herein the definition of (Born and Wolf 1991): $R_n^m(1) = 1$. Among many properties verified by these polynomials, we focus on:

$$\int_0^1 r R_n^m(r) J_m(vr) dr = (-1)^{\frac{n-m}{2}} \frac{J_{n+1}(v)}{v} \quad (A2)$$

see (Born and Wolf 1991, appendix VII) for the proof. This equality allows straightforward computation of the Fourier transform of the Zernike polynomials. In fact recall first that when $f(r, \theta) = g(r) \cos(m\theta)$, $m \in \mathbb{Z}$, a simple change of variables in the Fourier transform integral leads to:

$$\hat{f}(\rho, \phi) = 2\pi(-j)^m \cos(m\phi) \int_0^\infty r g(r) J_m(2\pi r \rho) dr \quad (A3)$$

An analog result for the inverse Fourier transform of $\hat{f}(\rho, \phi) = h(\rho) \cos(m\phi)$ is:

$$f(r, \theta) = 2\pi j^m \cos(m\theta) \int_0^\infty \rho h(\rho) J_m(2\pi r \rho) d\rho \quad (A4)$$

Applying the result of Eq. (A3) with Eq. (A2) immediately gives:

$$\widehat{U}_n^m(\rho, \phi) = j^m (-1)^{\frac{n+m}{2}} \cos(m\phi) \frac{J_{n+1}(2\pi\rho)}{\rho} \quad (\text{A5})$$

$$\widehat{U}_n^{-m}(\rho, \phi) = j^m (-1)^{\frac{n+m}{2}} \sin(m\phi) \frac{J_{n+1}(2\pi\rho)}{\rho} \quad (\text{A6})$$

The previous equation gives the inverse Fourier transform of $\cos(m\phi) \frac{J_{n+1}(2\pi\rho)}{\rho}$ when $n \geq m \geq 0$ and n et m share the same parity. In the general case where $n \geq 0$ and $m \geq 0$ this inverse Fourier transform, denoted as $f(r, \theta)$ must be computed independently. If we substitute $h(r)$ by $J_{n+1}(2\pi\rho)/\rho$ in Eq. (A4) the resulting integral is a Weber-Schafheitlin type integral (Abramowitz and Stegun 1972). This results in $f(r, \theta) = j^m \cos(m\theta) \mathcal{R}_n^m(r)$ where:

$$\text{if } r < 1, \mathcal{R}_n^m(r) = r^m \frac{\Gamma\left(\frac{n+m}{2} + 1\right)}{\Gamma(m+1)\Gamma\left(\frac{n-m}{2} + 1\right)} F\left(\frac{n+m}{2} + 1, \frac{m-n}{2}; m+1, r^2\right) \quad (\text{A7})$$

$F(a, b; c; z)$ is the Gauss hypergeometric function, see (Gradshteyn et al. 2000):

$$F(a, b; c; z) = 1 + \frac{ab}{1!c}z + \frac{a(a+1)b(b+1)}{2!c(c+1)}z^2 + \dots \quad (\text{A8})$$

It is interesting to note from Eqs. (A7) and (A8) that if $b = (m-n)/2 \in \mathbb{Z}^-$ the sum in Eq. (A8) reduces to a polynomial in z of order $-(m-n)/2$. Consequently $\mathcal{R}_n^m(r)$ reduces to a polynomial with degree n which of course coincides up to $(-1)^{(m-n)/2}$ with $R_n^m(r)$ for $r \leq 1$. For this reason $\mathcal{R}_n^m(r)$ can be considered as a natural generalization of the Zernike polynomials. Note that, contrarily to the generalization proposed in (Myrick 1966) or (Wünsche 2005), this generalization is not a polynomial.

We now briefly give the principal results related to the Gegenbauer polynomials. See for example (Andrews et al. 1999) or (Abramowitz and Stegun 1972) for detailed properties. The Gegenbauer (or ultraspherical) polynomials, noted as $t \mapsto C_k^{(\nu)}(t)$ are defined as the coefficients of the power series expansion of $r \mapsto (1 - 2rt + r^2)^{-\nu}$:

$$\frac{1}{(1 - 2rt + r^2)^\nu} = \sum_{k=0}^{\infty} C_k^{(\nu)}(t) r^k$$

For example $C_k^{(1)}(t)$ gives the Chebyshev polynomial of the second kind $U_k(t)$:

$$C_k^{(1)}(\cos(\psi)) = \sum_{q=0}^k \cos((k-2q)\psi) \quad (\text{A9})$$

Among the numerous beautiful properties of the Gegenbauer polynomials, we focus on the expansion:

$$\frac{J_\nu(w)}{w} = 2^\nu \Gamma(\nu) \sum_{k=0}^{\infty} (k+\nu) \frac{J_{k+\nu}(r)}{r^\nu} \frac{J_{k+\nu}(\rho)}{\rho^\nu} C_k^{(\nu)}(\cos(\gamma)) \quad (\text{A10})$$

where $w = \sqrt{r^2 + \rho^2 - 2r\rho \cos(\gamma)}$.

REFERENCES

- Abramowitz, M. and Stegun, I.A.: 1972, *Handbook of Mathematical Functions*, Dover
- Aime, C.: 2003, in C. Aime and R. Soummer (eds.), *Astronomy with High Contrast Imaging*, pp 65–87, E.A.S Publications Series
- Aime, C. and Soummer, R.: 2004, in C. Aime and R. Soummer (eds.), *Astronomy with High Contrast Imaging II*, pp 89–101, E.A.S Publications Series
- Aime, C., Soummer, R., and Ferrari, A.: 2002, *Astronomy and Astrophysics*, Vol. 389, pp 334–344
- Aime, C. and Vakili, F. (eds.): 2006, *Direct Imaging of Exoplanets: Science & Techniques*, International Astronomical Union Colloquium 200, Cambridge University Press
- Andrews, G.-E., Askey, R., Roy, R., and Rota, G.-C.: 1999, *Special Functions*, Encyclopedia of Mathematics and its Applications, Cambridge University Press
- Born, M. and Wolf, E.: 1991, *Principle of Optics*, Pergamon Press
- Chatelain, F., Ferrari, A., and Tourneret, J.-Y.: 2006, IEEE ICASSP
- Ferrari, A., Carillet, M., Aime, C., Serradel, E. and Soummer, R.: 2005 International Astronomical Union Colloquium 200, Cambridge University Press.
- Gradshteyn, I. S., Ryzhik, I. M., Jeffrey, A., and Zwillinger, D.: 2000, *Table of Integrals, Series, and Products, Sixth Edition*, Academic Press
- Guyon, O. and Roddier, F.: 2000, in *SPIE Interferometry in Optical Astronomy*, Vol. 4006, pp 377–387
- Lloyd, J. and Sivaramakrishnan, A.: 2005, *The Astrophysical Journal*, Vol. 14, No. 3, pp 476–489
- Mahajan, V.: 1994, *Applied Optics*, Vol. 33, pp 8121–8124
- Myrick, D.: 1966, *J. SIAM Appl. Math.*, Vol. 14, pp 476–489
- Pawlak, M. and Liao, X.L.: 2002, *IEEE trans. on Information theory*, Vol. 48, pp 2736–2753
- Sivaramakrishnan, A., Soummer, R., Lloyd, A. S. J., Oppenheimer, B., and Makidon, R.: 2005, *The Astrophysical Journal*, Vol. 634, pp 1416–1422
- Slepian, D.: 1964, *The Bell System Technical Journal*, Vol. 43, pp 3009–3058
- Soummer, R.: 2005, *The Astrophysical Journal*, Vol. 618, pp 161–164
- Soummer, R., Aime, C., and Falloon, P.: 2003, *Astronomy and Astrophysics*, Vol. 397, pp 1161–1172
- Wünsche, A.: 2005, *J. Comput. Appl. Math.*, Vol. 174, pp 135–163

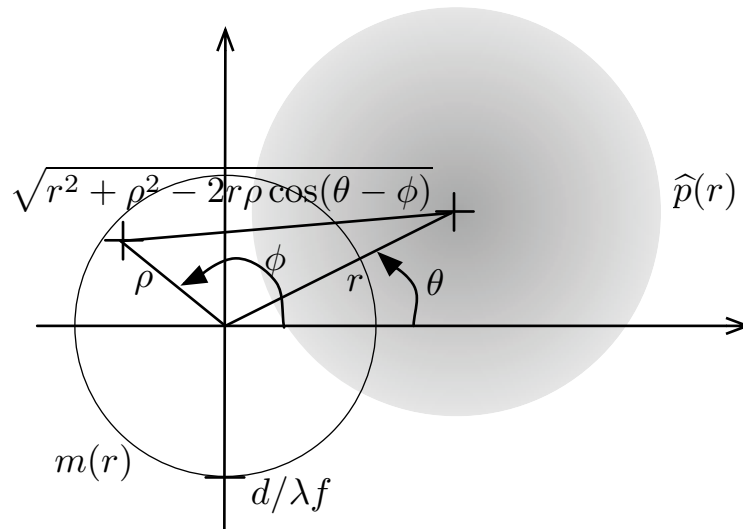


Fig. 1.— Computation of the convolution between $\widehat{\Psi}_A(r, \theta + \pi)m(r)$ and $\widehat{p}(r)$.

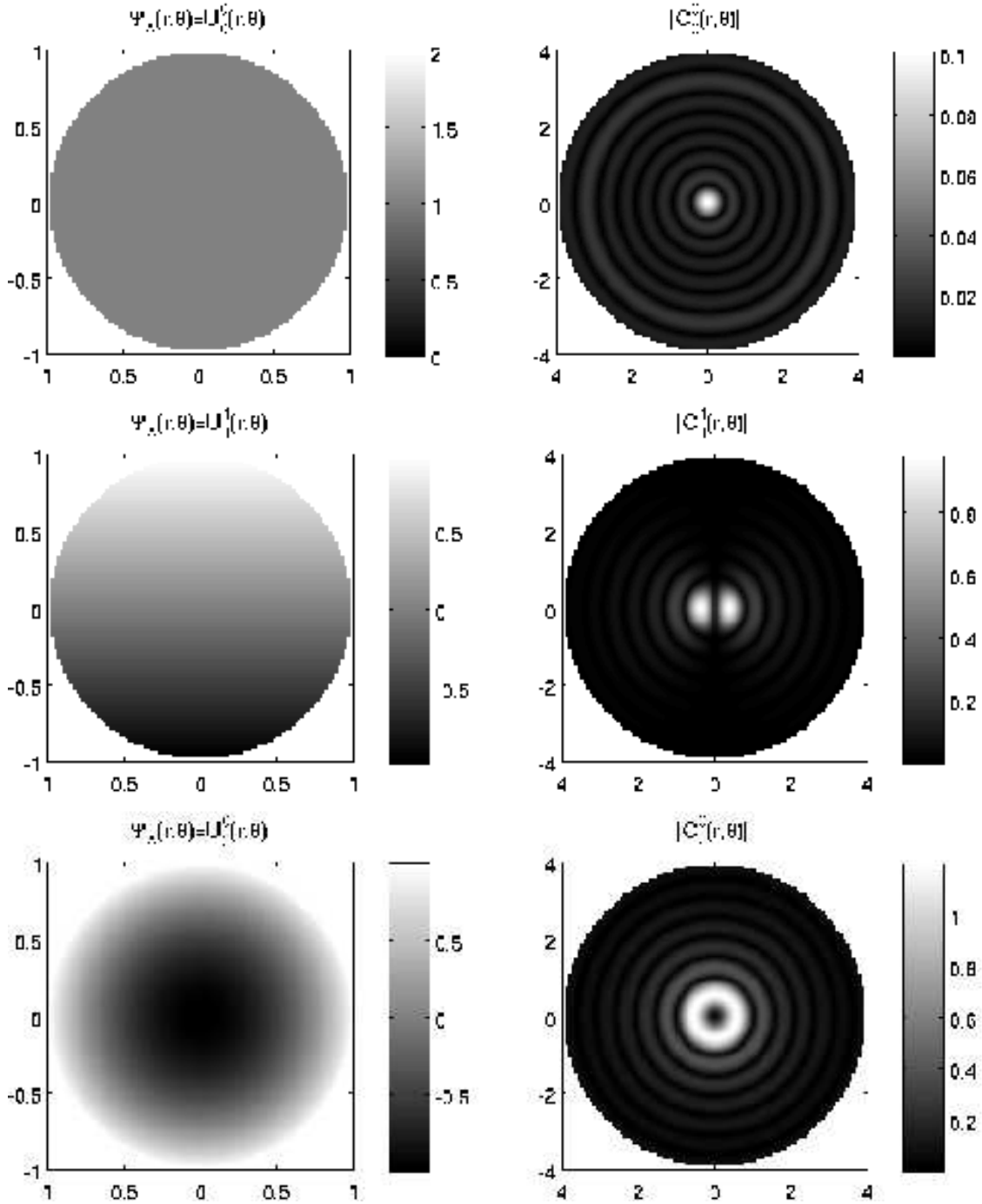


Fig. 2.— Complex amplitude in A and squared root of the amplitude in D , i.e. $|\mathcal{D}_n^m(r, \theta)|$. The parameters used in the simulation are: $\lambda f = 1$, $R = 1$, $d = 3$, $\epsilon = 1$ (Lyot coronagraph).

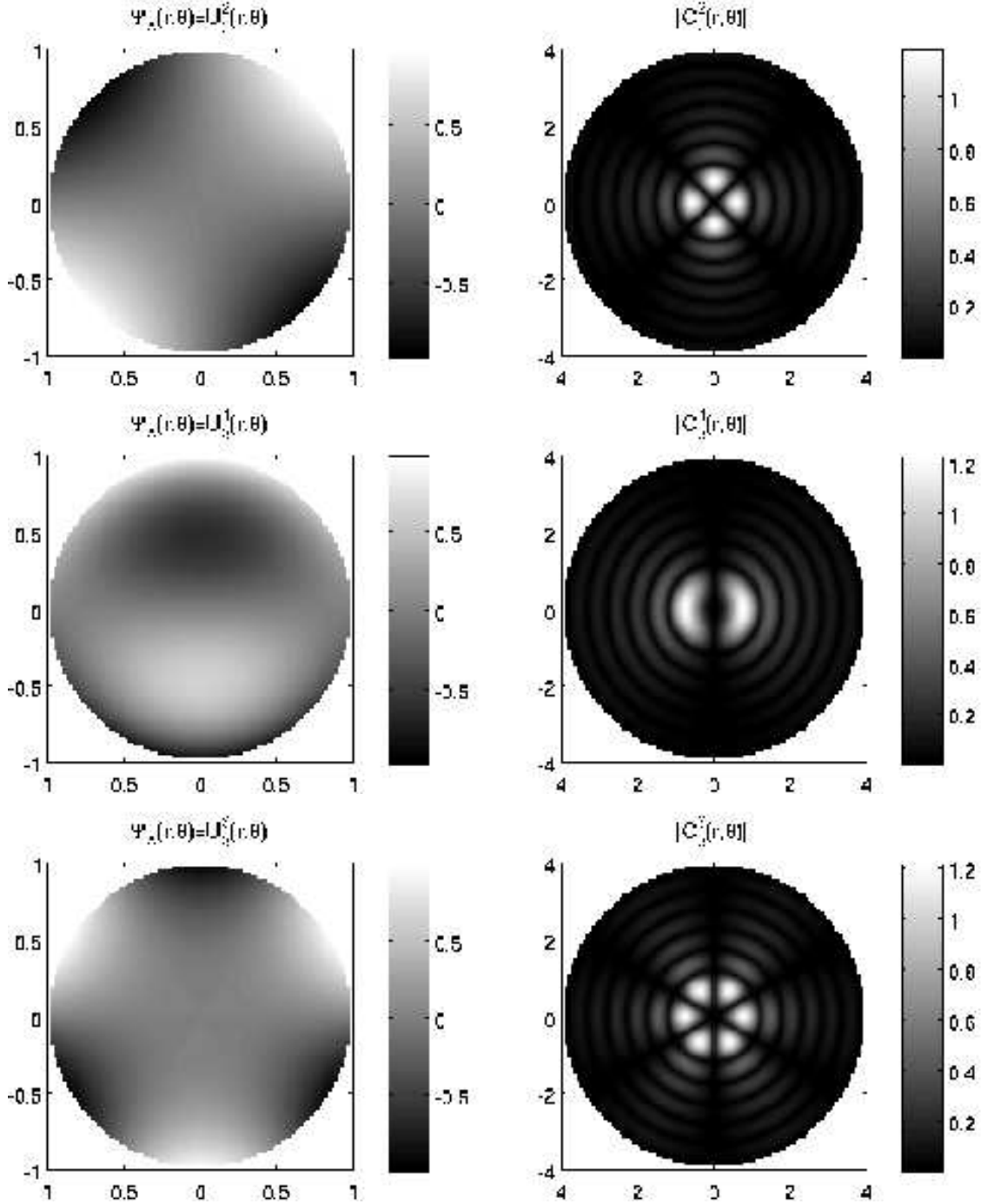


Fig. 3.— Complex amplitude in A and squared root of the amplitude in D , i.e. $|\mathcal{D}_n^m(r, \theta)|$. The parameters used in the simulation are: $\lambda f = 1$, $R = 1$, $d = 3$, $\epsilon = 1$ (Lyot coronagraph).

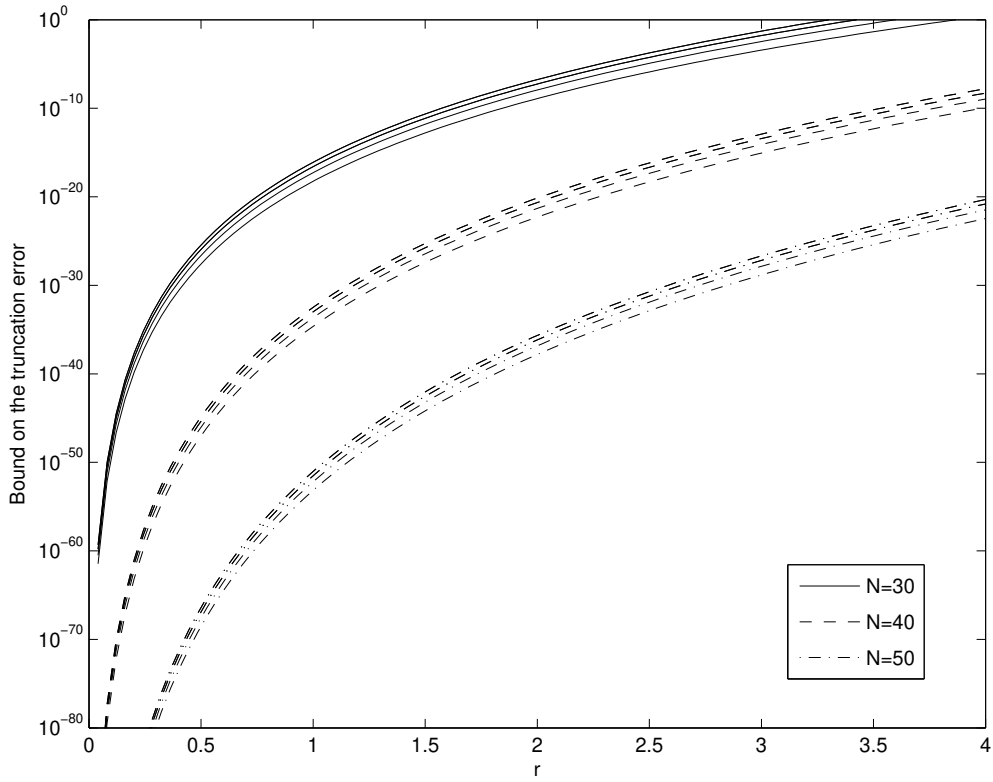


Fig. 4.— Bounds on the truncation error as a function of r . The parameters are the same as the parameters used for Figs. 2 and 3. For each value of N , the bound is plot for the first 6 Zernike polynomials.

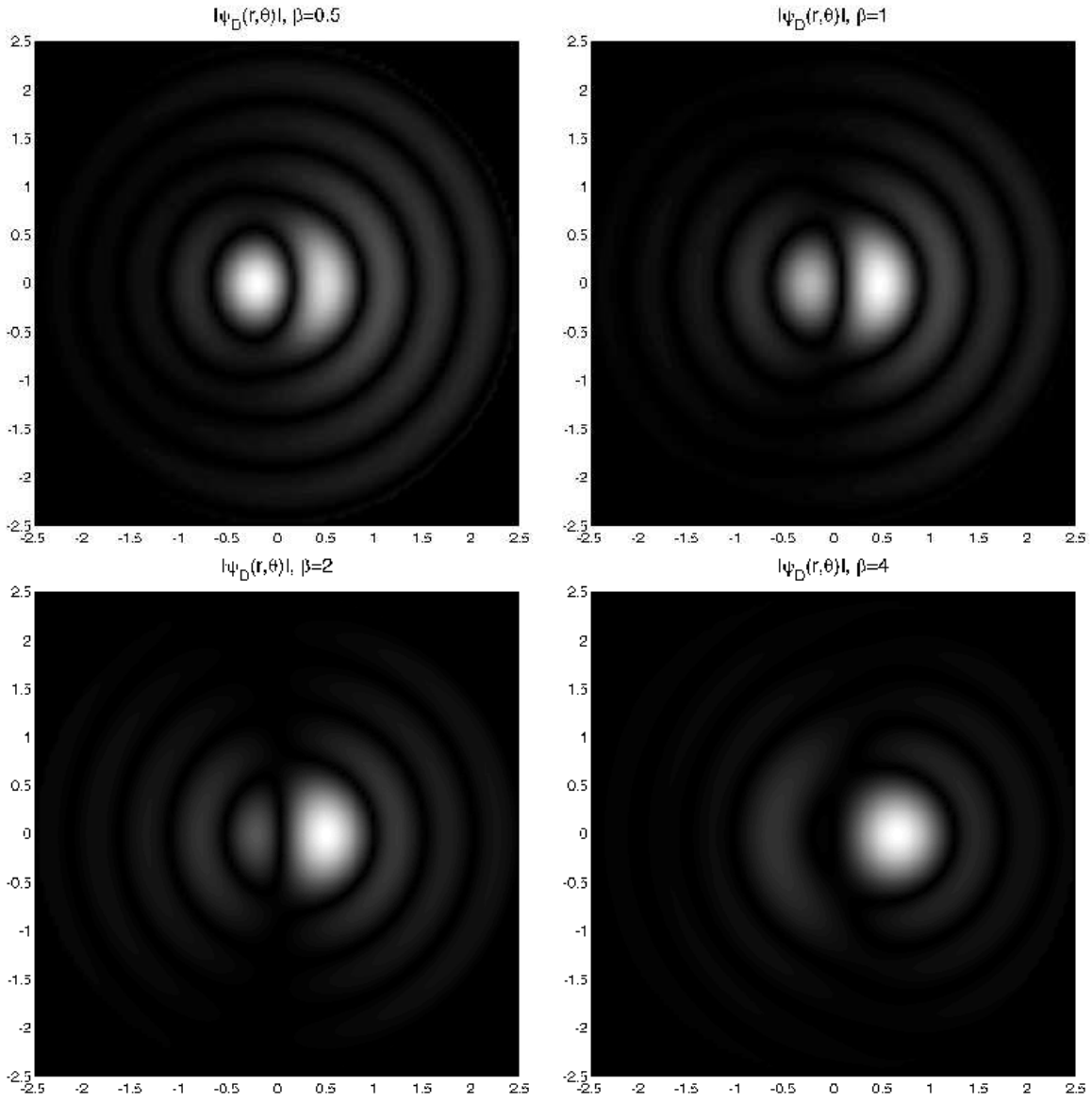


Fig. 5.— $|\Psi_D(r, \theta)|$ for different values of β . The parameters are the same as the parameters used for Figs. 2 and 3.